Electrochimica Acta 110 (2013) 228–233

Contents lists available at ScienceDirect

Electrochimica Acta

journal homepage: www.elsevier.com/locate/electacta

Manganese oxide/graphene oxide composites for high-energy aqueous asymmetric electrochemical capacitors

Charl J. Jafta[a,b,1], Funeka Nkosi[a,c], Lukas le Roux[a,2], Mkhulu K. Mathe[a,2], Mesfin Kebede[a], Katlego Makgopa[c], Yang Song[d], Dennis Tong[d], Munetaka Oyama[e,2], Ncholu Manyala[b], Shaowei Chen[d,**,2], Kenneth I. Ozoemena[a,c,*,2]

[a] Energy Materials, Materials Science and Manufacturing, Council for Scientific and Industrial Research (CSIR), Pretoria 0001, South Africa
[b] Department of Physics, Institute of Applied Materials, SARChI Chair in Carbon Technology and Materials, University of Pretoria, Pretoria 0002, South Africa
[c] Department of Chemistry, University of Pretoria, Pretoria 0002, South Africa
[d] Department of Chemistry and Biochemistry, University of California, Santa Cruz, CA 95064, USA
[e] Department of Material Chemistry, Graduate School of Engineering, Kyoto University, Nishikyo-ku, Kyoto 615-8520, Japan

ARTICLE INFO

Article history:
Received 30 November 2012
Received in revised form 10 June 2013
Accepted 15 June 2013
Available online 2 July 2013

Keywords:
Electrolytic manganese dioxide (EMD)
α-MnO_2
Graphene oxide
Asymmetric capacitor
Aqueous electrolyte
Energy density

ABSTRACT

A high-energy aqueous asymmetric electrochemical capacitor was developed using manganese dioxide (α-MnO_2)/graphene oxide (GO) nanocomposites. The nanostructured α-MnO_2 was prepared from micron-sized commercial electrolytic manganese dioxide (EMD) via a hydrothermal reaction in the presence and absence of sodium dodecylsulphate (SDS), α-$MnO_{2(SDS)}$ and α-MnO_2, respectively. Unlike the as-prepared α-MnO_2, the presence of SDS during the hydrothermal reaction conferred different morphologies on the intermediate precursors for the α-$MnO_{2(SDS)}$. Also, the XRD patterns showed that the α-$MnO_{2(SDS)}$ are more crystalline than the as-prepared α-MnO_2. The superior electrochemical performance of the α-$MnO_{2(SDS)}$/GO composite (280 $F g^{-1}$, 35 $Wh kg^{-1}$, and 7.5 $kW kg^{-1}$ at 0.5 $A g^{-1}$) coupled with excellent long cycle life clearly indicates that this electrode system has the potential of being developed as an efficient aqueous asymmetric electrochemical capacitor. The high performance of the α-$MnO_{2(SDS)}$/GO composite was interpreted in terms of the enhanced crystallinity of the α-$MnO_{2(SDS)}$. Interestingly, the electrochemical performance is comparable to or even better than those reported for the more conductive graphene/MnO_2 composites.

1. Introduction

Asymmetric electrochemical capacitors (ECs), also known as hybrid supercapacitors, are characterized by Faradaic reactions (pseudo-capacitance) and charge-storage (electrical double layer capacitance), and have begun to receive immense research interests because of their high energy density, large power density and long lifetime [1]. The use of aqueous electrolytes in asymmetric ECs is important due to several advantages of such systems [2], such as (i) simplicity of fabrication and packaging procedures that avoid rigorous environmental controls; (ii) a high degree of safety as compared to the use of organic-based ECs with respect to thermal stability and runaway; (iii) the use of low-toxicity and low-cost electrolytes; and (iv) specific energy that meets or exceeds those of non-aqueous EDLCs.

Toward this end, manganese dioxide (MnO_2) has been regarded as a promising active component for EC electrodes [3]. Electrolytic manganese oxide (EMD), on the other hand, does not show good capacitance. EMD is characterized by small surface areas and composed of a mixture of several crystallographic phases (α, β, γ, δ and λ). Of these, α-MnO_2 gives the best electrochemical capacitance [4]. South Africa has the largest manganese deposit in the world, and remains the major global supplier of EMD. One of the means of expanding the value chain of its manganese resource would be to find ways of exploiting EMD for energy storage systems. Therefore, there is a need to develop effective protocol whereby commercial EMD may be exploited to generate α-MnO_2 for electrochemical capacitor applications.

In addition, whereas activated carbons have been used extensively in the preparation of electrochemical capacitor electrodes [5–7], graphene and graphene oxide (GO) nanosheets are

* Corresponding author at: Energy Materials, Materials Science and Manufacturing, Council for Scientific and Industrial Research (CSIR), Pretoria 0001, South Africa. Tel.: +27 128413664; fax: +27 128412135.
** Corresponding author. Tel.: +1 831 459 5841; fax: +1 831 459 2935.
E-mail addresses: shaowei@ucsc.edu (S. Chen), kozoemena@csir.co.za (K.I. Ozoemena).
[1] ISE student member.
[2] ISE member.

0013-4686/$ – see front matter © 2013 Elsevier Ltd. All rights reserved.
http://dx.doi.org/10.1016/j.electacta.2013.06.096

beginning to be taunted as potential replacement due to their much enhanced energy densities. Theoretically, GO is not suitable for supercapacitor applications [8], but Xu et al. [9] recently showed that GO can exhibit higher capacitance than graphene due to the extra pseudo-capacitance effect of the attached oxygen-containing functional groups on its basal planes. Thus, in light of its higher capacitance, lower cost and shorter processing time than graphene, GO may become a better choice than graphene in electrochemical capacitor applications.

It is within such context that this study was carried out. In this communication we describe the properties of α-MnO_2/GO composite as a high-energy, high-power asymmetric electrochemical capacitor in neutral aqueous solutions. To our knowledge, this is the first study on the use of EMD-generated α-MnO_2/GO hybrids for asymmetric electrochemical capacitors in neutral aqueous electrolytes. We show that in aqueous electrolytes α-MnO_2/GO exhibits a high specific energy of 23–35 Wh kg^{-1} and high power density of 4.5–7.2 kW kg^{-1}, which are comparable to or even better than those reported for MnO_2/graphene asymmetric ECs reported in the literature [10–12]. In addition, the electrode shows excellent stability of over 1000 charge–discharge continuous cycles.

2. Experimental

2.1. Materials and procedure

Commercial electrolytic manganese dioxide (EMD) was obtained from a South African supplier, while sodium dodecylsulphate (SDS, 99%) was purchased from Sigma–Aldrich. The nanostructured α-MnO_2 was obtained from EMD via a hydrothermal reaction in the presence of SDS by slight modification of the literature method [13]. As summarized in Scheme 1, a mixture of 1 g of EMD, 1 g of SDS and 50 mL of 5% NH_4OH was stirred overnight and ultrasonicated for 30 min, transferred to a teflon-lined stainless steel beaker in an autoclave and heated at 130 °C for 24 h, then cooled to room temperature and washed several times with a copious amount of distilled water via centrifugation. The final product was dried overnight at 50 °C in a vacuum oven. These dried powders were then annealed at 620 °C for 2 h and subsequently subjected to an acid treatment to obtain the nanostructured α-$MnO_{2(SDS)}$. The acid treatment was carried out by reacting 10 mL of 8 M H_2SO_4 with 30 mg of the nanostructured Mn_2O_3 sample at ~100 °C for 6 h under continuous stirring, and then at room temperature for 16 h [13]. These samples were washed to a neutral pH with de-ionized water and then dehydrated at 300 °C to obtain the desired product. For comparison with the α-$MnO_{2(SDS)}$, another product (abbreviated herein as α-MnO_2) was obtained using the above method but without SDS.

GO was prepared using the modified Hummer's from graphite powders [14]. In brief, 0.5 g of graphite powders and 0.5 g of $NaNO_3$ were mixed with 23 mL of concentrated H_2SO_4 under magnetic stirring for 10 min in a clean flask at 0 °C. 3 g of $KMnO_4$ was then added slowly to the above solution over a 3 min period to prevent a sudden temperature increase. Then the dark greenish solution was transferred to a 35 ± 5 °C water bath and stirred for about 1 h. Next, 50 mL of water was added slowly, and the solution was stirred for another 30 min while the temperature was raised to 90 ± 5 °C. After adding 150 mL of water, 3 mL of H_2O_2 (30%) was added drop-wise, resulting in the formation of a brownish solution. Finally, the warm solution was filtered and washed with 50 mL of 0.1 M hydrochloric acid solution and 500 mL of water, respectively. The filter cake was then dispersed in water by sonication using a table-top ultrasonic cleaner (VWR B1500-A MTH, 50 W). The products were then separated via centrifugation for 5 min to remove all visible particles. The last sediment was re-dispersed in water under mild sonication, which resulted in a homogeneous brown solution of exfoliated

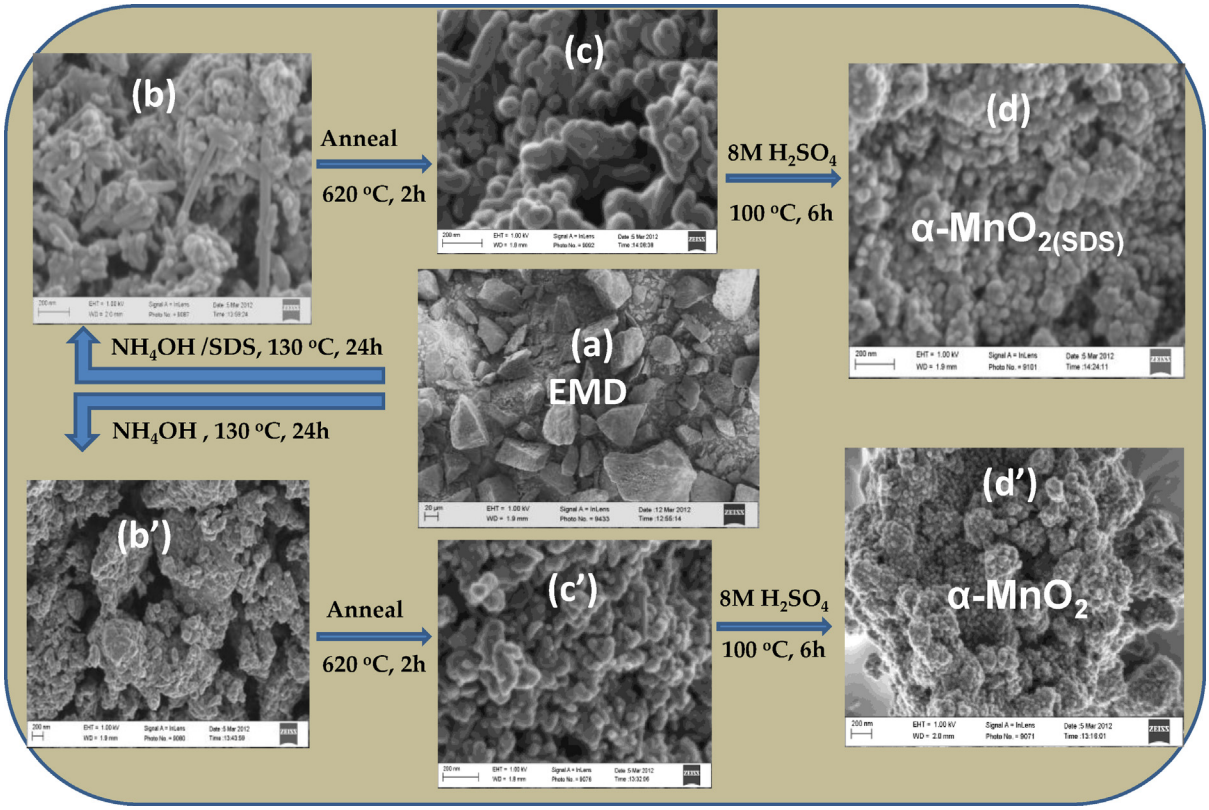

Scheme 1. The SDS-based and SDS-free routes for the preparation of α-$MnO_{2(SDS)}$ (d) and α-MnO_2 (d′) from EMD precursor (a) via intermediate nanostructures (b/b′) and (c/c′). Scale bars are 20 μm for (a), and 200 nm for structures (b/b′) to (d/d′).

GO. A ZEISS ULTRA SS (Germany) field emission scanning electron microscope (FESEM) was used to obtain the images of the prepared powders. The X-ray diffraction studies were carried out using a Bruker AXS D8 ADVANCE X-ray Diffractometer with Ni-filtered Cu Kα radiation (λ = 1.5406 Å). The X-ray tube operating parameters were 40 kV and 40 mA. The scanning speed was 0.02° per step with a dwell time of 5.0 s. GO samples were prepared for high resolution transmission electron microscopy (HR-TEM) by drop-casting a dilute (1 mg mL^{-1}) aqueous solution of graphene oxide onto a lacey carbon coated 400 mesh copper grids. The electron microscope was a modified Philips CM300FEG/UT operating at 300 kV.

2.2. Electrode fabrication and electrochemical testing

Electrochemical measurements were performed in a single-cell configuration using coin cells (LIR-2032). Prior to use, the current collector (nickel foam) was cleaned in a 1 M HCl solution, washed with a copious amount of de-ionized water, and dried under vacuum. A 1 M Li_2SO_4 solution served as the electrolyte while a glass microfiber served as the separator. The α-MnO_2/GO and α-$MnO_{2(SDS)}$/GO composites were obtained by milling α-MnO_2 or α-$MnO_{2(SDS)}$ with GO at a mass ratio of 85:15. The positive electrode (α-MnO_2/GO or α-$MnO_{2(SDS)}$/GO composites) was prepared by first mixing α-MnO_2/GO or α-$MnO_{2(SDS)}$/GO with carbon black (CB) and polyvinylidene fluoride (PVDF) at a mass ratio of 70:20:10 ($MnO_{2(SDS)}$/GO:CB:PVDF) using pestle and mortar and then dispersing a few drops of anhydrous N-methyl-2-pyrrolidone to produce a homogeneous paste. CB and PVDF served as the conductive agent and binder, respectively. The resulting slurry was coated onto the nickel foam substrate (~3 cm^2) with a spatula, with an average mass loading of ~1 mg/cm^2. The electrode was then dried at 80 °C for 8 h in a vacuum oven, and pressed to a thickness of ~0.5 mm. The negative electrode was prepared using the same procedure but with CB, GO and PVDF at a mass ratio of 80:10:10. The cell was tested after 24 h of fabrication. Cyclic voltammetry, galvanostatic charge-discharge measurements, and EIS were carried out using an Autolab potentiostat PGSTAT 302N (Eco Chemie, Utrecht, The Netherlands) driven by the General Purpose Electrochemical Systems data processing software (GPES and FRA software version 4.9).

3. Results and discussion

3.1. SEM and XRD characterization

As summarized in Scheme 1, the SDS-based and SDS-free routes show different morphologies of the intermediate products (b/b′ and c/c′). While the SDS-based intermediates were needle-like (b) and rod-like (c) nanostructures, their SDS-free counterpart (b′and c′) were nanoparticles. The final products (d and d′) gave essentially similar morphology. The results clearly prove that SDS confer different morphology during the nanostructuring process of the raw EMD. As the EMD and SDS mixture was thoroughly stirred and ultrasonicated for long periods of time prior to hydrothermal treatment, it can be assumed that the distribution of SDS was sufficiently uniform. Considering that the final SDS-based product was subjected to high temperature annealing (620 °C) it means that any 'unreacted SDS' would have been completely burnt off during this heat treatment. Thus, the addition of SDS (an anionic surfactant) during synthesis only served to enhance the disaggregation of the bulky EMD and confer needle-like or rod-like intermediate nanostructures that permit the enhanced crystallinity of the final product.

To examine the impact of the SDS on the crystal structures of the final products, XRD analyses were performed. Fig. 1 shows the

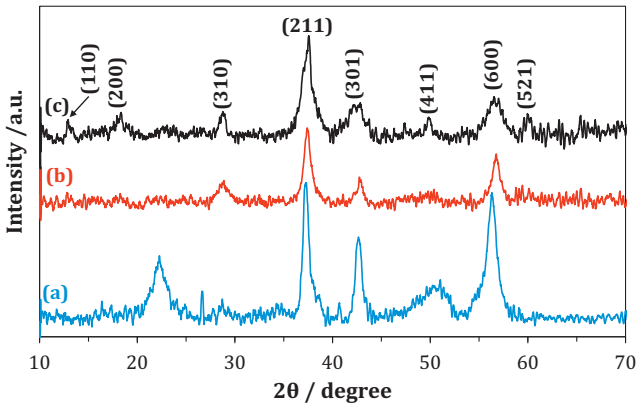

Fig. 1. X-ray diffraction patterns of EMD (a), α-MnO_2 (b), and α-$MnO_{2(SDS)}$ (c).

XRD patterns of EMD (a), α-MnO_2 (b) and α-$MnO_{2(SDS)}$ (c). In contrast to EMD, the XRD patterns of the transformed α-MnO_2, both in the absence and presence of the surfactant SDS, show peaks that can be indexed to tetragonal α-MnO_2 (JCPDS 44-0141). In addition, it is evident from Fig. 1 that α-$MnO_{2(SDS)}$ is more crystalline than α-MnO_2 as the (1 1 0), (2 0 0), (4 1 1) and (5 2 1) reflections are much better-defined. Also, the peaks in the former are somewhat broader, signifying the formation of smaller crystallites. Using the (2 1 1) reflection of patterns (b, α-MnO_2) and (c, α-$MnO_{2(SDS)}$) the average particle sizes were calculated using the Scherrer equation, $D = 0.9\lambda/\beta\cos\theta$. The calculated particle sizes were ca. 20.9 and 11.8 nm for α-MnO_2 and α-$MnO_{2(SDS)}$, respectively.

A graphene oxide sheet obtained by the modified Hummer's method [14] is shown in Fig. 2. The smooth sheet may be identified in the micrograph, while the edges tend to fold and roll. Lattice fringes are visible on the edges of graphene oxide sheets due to folds and/or rolls, as can be seen in the HRTEM image in Fig. 2. The separation between neighboring fringes (Fig. 2 inset) was measured to be ~0.37 nm and is larger than the inter-planar spacing in graphite (0.335 nm) [15], which can be attributed to the presence of oxygen functional groups on the graphene oxide layers.

3.2. Cyclic voltammetric characterization

Cyclic voltammograms recorded for the α-MnO_2/GO and α-$MnO_{2(SDS)}$/GO at a potential sweep rate of 15 mV s^{-1} are presented in Fig. 3. Both α-MnO_2/GO and α-$MnO_{2(SDS)}$/GO showed capacitive behavior with absolute operating voltage windows of 2.0 and ~1.8 V, respectively. The α-$MnO_{2(SDS)}$/GO showed high current response at the two extreme voltages which may be due to hydrogen and oxygen evolution reactions within the cell. It seems that the MnO_2 made via SDS route conferred on the MnO_2 catalytic properties for H_2 and O_2 evolution. Further work will be necessary to explore this phenomenon. The current response of the SDS coated sample is superior when compared to the sample without surfactant indicating that the α-$MnO_{2(SDS)}$/GO sample has a better capacitance.

3.3. Galvanostatic charge-discharge experiment

The supercapacitive performance properties were evidenced by the galvanostatic charge–discharge experiments, as exemplified in Fig. 4. The absolute operating voltage windows are in agreement with the CV data. The specific capacitance (C_{sp}), maximum specific power density (P_{max}) and specific energy density (E_{sp}) were

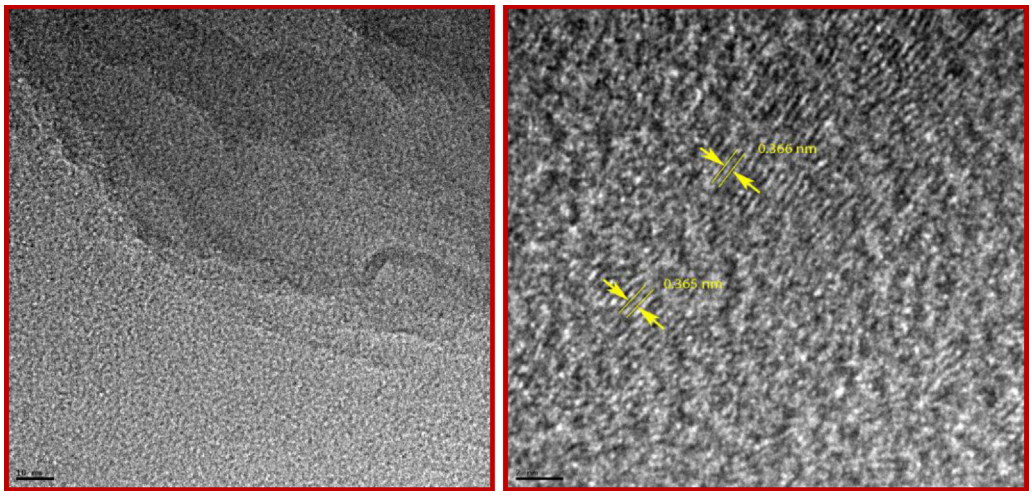

Fig. 2. Representative HRTEM images of graphene oxide. Scale bars are 10 nm and 2 nm in the left and right panel, respectively.

determined from the discharge curves using the established Eqs. (1)–(4) for a 2-electrode device [16,17]:

$$C(F) = \frac{i}{\Delta V/\Delta t} \quad (1)$$

$$C_{sp}(\mathrm{F\ g^{-1}}) = \frac{4C}{m} \quad (2)$$

$$E(\mathrm{W\ h\ kg^{-1}}) = \frac{CV^2}{2m} \quad (3)$$

$$P_{max}(\mathrm{W\ kg^{-1}}) = \frac{V^2}{4R_{ir}m} \quad (4)$$

where i (A) is the applied current, ΔV (V)/Δt (s) the slope of the discharge curve after the initial iR drop and m (g) the mass of both electrodes. In this work, the mass was considered to be that of the active material (α-MnO_2/GO, GO or EMD). V (V) is the maximum voltage obtained during charge and C (F) the calculated capacitance. The internal resistance (R_{ir}) can be calculated from the voltage drop at the beginning of a discharge curve:

$$R_{ir}(\Omega) = \frac{\Delta V_{iR}}{2i} \quad (5)$$

where ΔV_{iR} is the voltage drop between the first two points from the start of the discharge curve. The first three charge–discharge cycles for EMD/GO show a surprisingly good capacitance of 76.9 F g^{-1} for this micron-sized material. However, after the initial three cycles, the capacitance degenerated rapidly, thus no further experiment was performed with this electrode. It is noted that the specific capacitance of the α-MnO_2/GO and α-$MnO_{2(SDS)}$/GO can reach 153.1 F g^{-1} and 279.8 F g^{-1}, respectively, at a current density of 0.5 A g^{-1}, as shown in Table 1. Fig. 4(b) shows the stability of α-MnO_2/GO and α-$MnO_{2(SDS)}$/GO when cycled at a current density of 1 A g^{-1} for 1000 cycles. There is a 44% and 30% decrease in the capacitance in the first 50 cycles for the

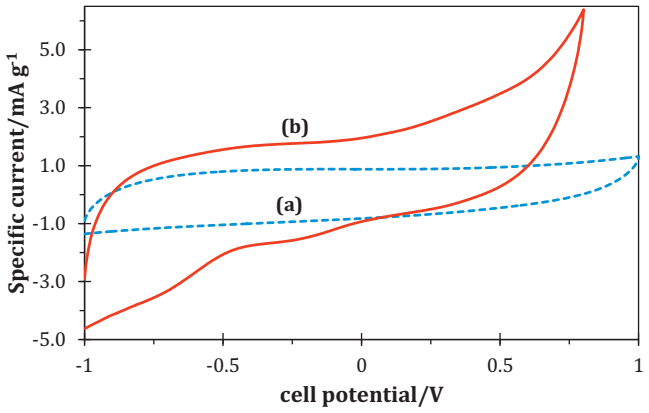

Fig. 3. Cyclic voltammograms of the α-MnO_2/GO (a) and that of the α-$MnO_{2(SDS)}$/GO (b) at a scan rate of 15 mV s^{-1}.

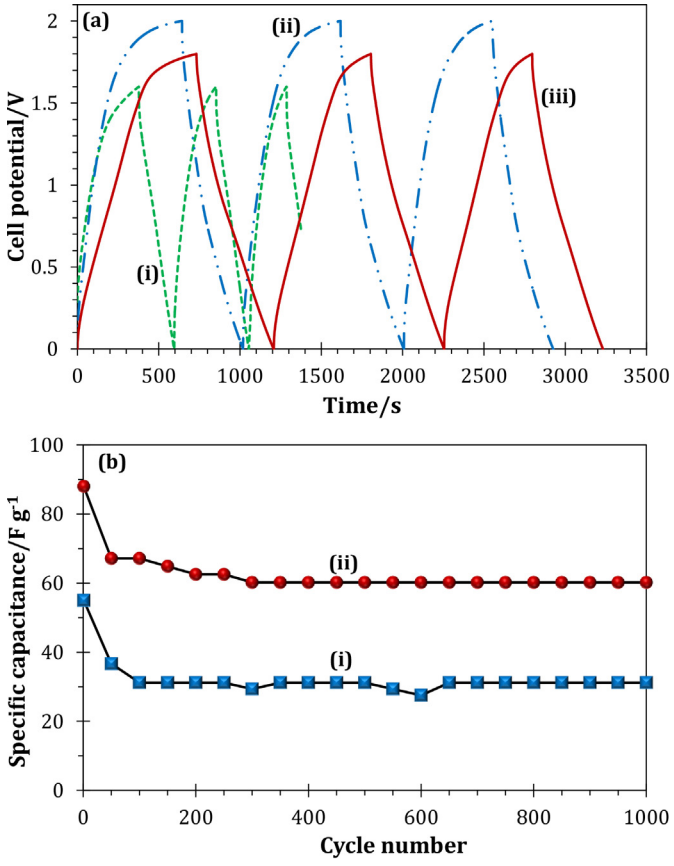

Fig. 4. (a) Galvanostatic charge–discharge curves of EMD/GO (i), α-MnO_2/GO (ii) and α-$MnO_{2(SDS)}$/GO (iii), and (b) the cycle stability of the α-MnO_2/GO (i) and α-$MnO_{2(SDS)}$/GO (ii).

Table 1
Comparative performance of some manganese oxide based aqueous asymmetric electrochemical capacitors.

Electrode	Electrolyte	V_{max}(V)	C_{sp}(F g^{-1})	E_{sp} (Wh kg^{-1})	P_{max} (kW kg^{-1})	Ref.
EMD/GO	1 M Li_2SO_4	1.6	77	10.4	2.7	This work
α-MnO_2/GO	1 M Li_2SO_4	2.0	153	23.6	4.5	This work
α-$MnO_{2(SDS)}$/GO	1 M Li_2SO_4	1.8	280	35.0	7.2	This work
MnO_2 nw/G	1 M Na_2SO_4	2.0	30	30.4	5	[12]
MnO_2-textile/G	0.5 M Na_2SO_4	1.0	315	12.5	110	[10]
MnO_2/AC	2 M KNO_3	2.0	140	21	123	[21]

Key: GO, graphene oxide; G, graphene; nw, nanowire; AC, activated carbon; SDS, sodium dodecylsulphate.

α-MnO_2/GO and α-$MnO_{2(SDS)}$/GO, respectively, after which the capacitance remained constant throughout the cycling period. Fig. 5 compare the energy and power densities (Ragone plot) of EMD/GO, α-MnO_2/GO and α-$MnO_{2(SDS)}$/GO. The energy density of α-$MnO_{2(SDS)}$/GO is apparently higher with a value of 35 Wh kg^{-1}.

The enhanced capacitive energy storage properties of the SDS-based α-MnO_2 nanoparticles should perhaps not be surprising since good crystallinity should improve the electrochemistry. For example, Ghodbane et al. [18] demonstrated that the crystallographic structure has a significant influence on the capacitive storage behavior of MnO_2. Mao et al. [19] recently showed that a composite of needle-like α-MnO_2 and tetrabutylammonium hydroxide stabilized graphene (α-MnO_2/GTR) with good crystallinity showed better capacitive energy storage performance compared with the other two systems with poor crystallinity. Kim et al. [20] proved that high crystallinity greatly improved the electrochemistry and rapid pseudocapacitive response of Nb_2O_5.It is worth mentioning that, to the best of our knowledge, there is no literature report on the use of GO with MnO_2 to prepare supercapacitors in a two-electrode cell (asymmetric cell). The α-$MnO_{2(SDS)}$/GO prepared above showed excellent stability upon continuous cycling (1000 cycles), with > 70% capacity retention. The energy deliverable efficiency (η/%) was obtained from equation (6)

$$\eta(\%) = \frac{t_d}{t_c} \times 100 \quad (6)$$

where t_d and t_c are the total amount of discharge and charging times, respectively. The energy deliverable efficiency of α-$MnO_{2(SDS)}$/GO was ≥97%. The stability study proves that both the α-MnO_2/GO and α-$MnO_{2(SDS)}$/GO can charge and discharge continuously without significant deterioration in efficiency. The improved performance of this electrode is due to the pseudocapacitance arising from the oxygenated groups at the GO. Also, although GO is an insulating material, with a conductivity in the 10^{-6} S m^{-1} order, which is several orders of magnitudes lower than that of graphene. However, as shown by Xu et al. [9] after pressing them into membrane electrodes with carbon black as a conductive additive, the conductivities of the electrodes containing graphene oxide is greatly improved.

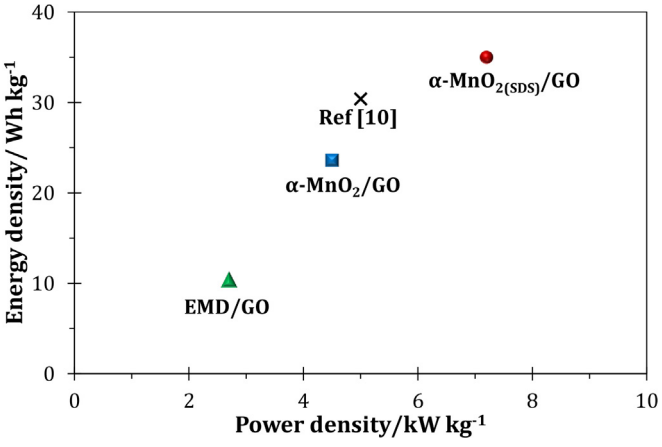

Fig. 5. Ragone plot comparing the energy and power densities of the EMD/GO, α-MnO_2/GO and α-$MnO_{2(SDS)}$/GO.

4. Conclusions

The electrochemical properties of nanostructured α-MnO_2/graphene oxide composite have been reported for application in aqueous asymmetric electrochemical capacitor. The addition of the surfactant (SDS) during the synthesis of α-MnO_2 from a multi-phased electrolytic manganese dioxide led to a significant enhancement on the electrochemical performance of the α-MnO_2/graphene oxide nanocomposite. In the electrochemical measurements, the addition of SDS during the synthesis of α-MnO_2 improved the cell conductivity and capacitive energy storage. The high energy density (35 Wh kg^{-1}) coupled with long-term cycling stability, clearly indicate that this nanomaterial may be useful for future development of low-cost asymmetric electrochemical capacitor.

Acknowledgements

C.J.J. thanks the CSIR for the doctoral studentship. We thank the CSIR, University of Pretoria, and NRF (K.I.O), and the US National Science Foundation (CHE-1012258 and DMR-0804049, S.W.C.) for supporting this work.

References

[1] R. Kötz, M. Carlen, Principles and applications of electrochemical capacitors, Electrochimica Acta 45 (2000) 2483.
[2] J.W. Long, D. Bélanger, T. Brousse, W. Sugimoto, M.B. Sassin, O. Crosnier, Asymmetric electrochemical capacitors—Stretching the limits of aqueous electrolytes, MRS Bulletin 36 (2011) 513.
[3] V. Subramanian, H. Zhu, B. Wei, Nanostructured MnO_2: Hydrothermal synthesis and electrochemical properties as a supercapacitor electrode material, Journal of Power Sources 159 (2006) 361.
[4] S. Devaraj, N. Munichandraiah, Effect of crystallographic structure of MnO_2 on its electrochemical capacitance properties, Journal of Physical Chemistry C 112 (2008) 4406.
[5] E. Frackowiak, F. Béguin, Carbon materials for the electrochemical storage of energy in capacitors, Carbon 39 (2001) 937.
[6] E. Frackowiak, F. Béguin, Electrochemical storage of energy in carbon nanotubes and nanostructured carbons, Carbon 40 (2002) 1775.
[7] L.L. Zhang, X. Zhao, Carbon-based materials as supercapacitor electrodes, Chemical Society Reviews 38 (2009) 2520.
[8] Y. Wang, Z. Shi, Y. Huang, Y. Ma, C. Wang, M. Chen, Y. Chen, Supercapacitor devices based on graphene materials, Journal of Physical Chemistry C 113 (2009) 13103.
[9] B. Xu, S. Yue, Z. Sui, X. Zhang, S. Hou, G. Cao, Y. Yang, What is the choice for supercapacitors: graphene or graphene oxide? Energy & Environmental Science 4 (2011) 2826.

[10] G. Yu, L. Hu, M. Vosgueritchian, H. Wang, X. Xie, J.R. McDonough, X. Cui, Y. Cui, Z. Bao, Solution-processed graphene/MnO_2 nanostructured textiles for high-performance electrochemical capacitors, Nano Letters 11 (2011) 2905.
[11] G. Yu, L. Hu, N. Liu, H. Wang, M. Vosgueritchian, Y. Yang, Y. Cui, Z. Bao, Enhancing the Supercapacitor Performance of Graphene/MnO_2 Nanostructured Electrodes by Conductive Wrapping, Nano Letters 11 (2011) 4438.
[12] Z.S. Wu, W. Ren, D.W. Wang, F. Li, B. Liu, H.M. Cheng, High-energy MnO_2 nanowire/graphene and graphene asymmetric electrochemical capacitors, ACS Nano 4 (2010) 5835.
[13] C.S. Johnson, D.W. Dees, M.F. Mansuetto, M.M. Thackeray, D.R. Vissers, D. Argyriou, C.-K. Loong, L. Christensen, Structural and electrochemical studies of α-manganese dioxide (α-MnO_2), Journal of Power Sources 68 (1997) 570.
[14] W.S. Hummers Jr., R.E. Offeman, Preparation of graphitic oxide, Journal of the American Chemical Society 80 (1958) 1339.
[15] H.P. Boem, Carbon Surface Chemistry in Graphite and Precursors, 1st ed., Gordon and Breach Science Publishers, France, 2001.
[16] X. Zhao, L. Zhang, S. Murali, M.D. Stoller, Q. Zhang, Y. Zhu, R.S. Ruoff, Incorporation of Manganese Dioxide within Ultraporous Activated Graphene for High-Performance Electrochemical Capacitors, ACS Nano 6 (2012) 5404.
[17] J. Duay, E. Gillette, R. Liu, S.B. Lee, Highly flexible pseudocapacitor based on free-standing heterogeneous MnO_2/conductive polymer nanowire arrays, Physical Chemistry Chemical Physics 14 (2012) 3329.
[18] O. Ghodbane, J. Pascal, F. Favier, Microstructural effects on charge-storage properties in MnO_2-based electrochemical supercapacitors, ACS Applied Materials & Interfaces 1 (2009) 1130.
[19] L. Mao, K. Zhang, H.S.O. Chan, J. Wu, Nanostructured MnO_2/graphene composites for supercapacitor electrodes: the effect of morphology, crystallinity and composition, Journal of Materials Chemistry 22 (2012) 1845.
[20] J.W. Kim, V. Augustyn, B. Dunn, The Effect of Crystallinity on the Rapid Pseudocapacitive Response of Nb_2O_5, Advanced Energy Materials 2 (2012) 141.
[21] V. Khomenko, E. Raymundo-Pinero, F. Béguin, Optimisation of an asymmetric manganese oxide/activated carbon capacitor working at 2V in aqueous medium, Journal of Power Sources 153 (2006) 183.